Journal of Sound and Vibration (1997) **201**(5), 555–565

THERMODYNAMIC DAMPING IN POROUS MATERIALS WITH ELLIPSOIDAL CAVITIES

S. D. PANTELIOU†

Department of Mechanical Engineering, University of Patras, Patras 26110, *Greece*

AND

A. D. DIMAROGONAS

W. Palm Professor of Mechanical Design, Washington University, St. Louis, MO 63130, *U.S.A.*

(*Received* 1 *July* 1996, *and in final form* 2 *October* 1996)

When a material is subjected to an alternating stress field, there are temperature fluctuations throughout its volume due to thermoelastic effects. The resulting irreversible heat conduction leads to entropy production which, in turn, is the cause of thermodynamic damping. An analytical investigation of the entropy produced during a vibration cycle due to the reciprocity of temperature rise and strain yielded the change of the material damping factor as a function of shape and magnitude of the porosity of the material. A homogeneous, isotropic, elastic bar of cylindrical shape is considered with uniformly distributed ellipsoidal cavities under alternating uniform axial stress. The analytical calculation of the dynamic characteristics of the porous structure yielded the change of the material damping factor as a function of shape and magnitude of the porosity of the material. A homogeneous, isotropic, elastic bar of cylindrical shape is considered with uniformly distributed ellipsoidal cavities under alternating uniform axial stress. The analytical calculation of the dynamic characteristics of the porous structure yielded the damping factor of the bar and the material damping factor. Experimental results on porous metals are in good correlation with analysis.

1. INTRODUCTION

It is well known that the porosity in a material is related to the decrease in its strength. The evaluation of the effect of inclusions on the strength of a material, especially in relation to fatigue and brittle fracture, is a very important consideration in engineering design.

Damping is also a very important material property when dealing with vibrating structures from the point of view of vibration isolation in many applications: bearings, filters, aircraft parts, and generally structures made of porous materials. For a material there are many damping mechanisms [1], most of which contribute significantly to the total damping only over a certain narrow range of frequency, temperature or stress. Thermodynamic damping is due to the irreversible heat conduction in the material.

Thermodynamic damping was first studied by Zener [2], for transverse vibrations of a homogeneous Euler–Bernoulli beam. The case of a general homogeneous medium was investigated by Biot [3], Lucke [4], Deresiewicz [5], Alblas [6, 7] and Gillis [8], while the cases of homogeneous plates, shells and Timoshenko beams were investigated by Tasi [9], Tasi and Herrmann [10], Shieh [11–13] and Lee [14]. The connection between the second law of thermodynamics and thermodynamic damping was also discussed by Goodman *et al*. [15] and by Landau and Lifshitz [16]. Armstrong [17] calculated the thermodynamic

†Present address, Department of Mechanical Engineering, Washington University, St Louis, MO 63130, U.S.A.

0022–460X/97/150555 + 11 $25.00/0/sv960784

damping of a one-dimensional composite consisting of successive slabs assuming identical thermal conductivity and specific heat for all slabs. Kinra and Milligan [18] presented a general methodology for calculating thermodynamic damping in homogeneous or composite materials. Milligan and Kinra [19] extended the calculation to a single linear inclusion in an unbounded matrix. The case of an Euler–Bernoulli beam was examined by Bishop and Kinra [20]. Bishop and Kinra [21], also investigated the thermodynamic damping of a laminated beam in flexure and extension, and further [22] calculated the thermodynamic damping of an N-layer metal matrix composite in Cartesian, cylindrical and spherical co-ordinates systems with perfect or imperfect thermal interfaces. Milligan and Kinra [23] calculated the thermodynamic damping of a fiber reinforced metal–matrix composite.

In this paper the thermodynamic damping of a homogeneous, isotropic, elastic bar with uniformly distributed ellipsoidal cavities under alternating uniform axial stress is calculated analytically and determined experimentally.

2. ANALYTICAL MODEL

The thermomechanical behaviour of a linear, isotropic and homogeneous thermoelastic medium is described by the following equations: the first law of thermodynamics [24],

$$\rho\partial u/\partial t = \sigma_{ij}\partial e_{ij}/\partial t - q_{i,i}; \tag{1}$$

Newton's law of motion–conservation of linear momentum [25],

$$\sigma_{ji,j} = \rho\partial^2 u_i/\partial t^2; \tag{2}$$

the kinematic equations of linear thermoelasticity-strain displacement relations [26],

$$e_{ij} = 1/2(u_{i,j} + u_{j,i}); \tag{3}$$

the second law of thermodynamics [24],

$$\rho\partial s/\partial t + (q_i/T)_i \geqslant 0; \tag{4}$$

the thermoelastic Hooke's law [26],

$$\sigma_{ij} = E/(1+v)(e_{ij} + v/(1-2v)e_{kk}\delta_{ij}) - E/(1-2v)\alpha_1\delta_{ij}(T - T_0); \tag{5}$$

the Fourier law of heat conduction [27],

$$q_i = -kT_{,i}. \tag{6}$$

Here σ_{ij} is the stress tensor, e_{ij} is the strain tensor, u_i is the displacement vector, v is the Poisson ratio, E is the Young modulus, ρ is the density, s is the entropy produced per unit mass, T is the absolute temperature, T_0 is the thermodynamic equilibrium temperature, q_i is the heat flux vector, u is the internal energy per unit mass, δ_{ij} is the Kronecker delta, k is the thermal conductivity, α_1 is the coefficient of thermal expansion, and the indices i,j, and k each have values of 1, 2, and 3.

From these equations the relation between temperature and strain is [25]

$$T_{,ii} - (\rho c/k)\partial T/\partial t = [E\alpha_1/k(1-2v)]T\partial e_{kk}/\partial t. \tag{7}$$

In this equation the term $(T\partial e_{kk}/\partial t)$ couples the temperature field with the mechanical field and leads to a non-linear problem. One can replace T on the right side of equation (7) by the thermodynamic equilibrium temperature T_0, because the fluctuations in temperature caused by reasonable alternating stress levels are very small. This assumption linearizes

the differential equation. Equation (7) shows that, for an isotropic material [28],

$$(\partial T/\partial \sigma_{kk})_s = -T\alpha_1/C, \tag{8}$$

where C is the specific heat per unit volume. Since the temperature and mechanical fields are coupled, inhomogeneities in stress and material properties result in inhomogeneities in temperature. Heat is conducted from the high temperature regions to the low temperature regions and, as consequence of the second law of thermodynamics, entropy is produced which is manifested as a conversion of useful mechanical energy into heat.

When the second law of thermodynamics is applied to heat conduction in solids, it results in the calculation of the flow of entropy produced per unit volume, $\dot{s}_p = \mathrm{d}s_p/\mathrm{d}t$ due to irreversible heat conduction [29, 30]:

$$\dot{s}_p = k/(\rho T_0^2)(\partial T/\partial r)^2, \tag{9}$$

The elastic energy W_{el} stored per unit volume and cycle of vibration is [31]

$$W_{el} = (1/2E)(\sigma_{rr}^2 + \sigma_{zz}^2 + \sigma_{\theta\theta}^2) - (v/E)(\sigma_{rr}\sigma_{zz} + \sigma_{zz}\sigma_{\theta\theta} + \sigma_{\theta\theta}\sigma_{rr}). \tag{10}$$

The entropy Δs produced per unit volume and cycle of vibration is

$$\Delta s = \oint_T \dot{s}_p \, \mathrm{d}t, \tag{11}$$

where T_p is the period of vibration.

From the Gouy–Stodola theorem [32–34] the mechanical energy $\dot{W}$ dissipated per unit of volume and per unit of time is

$$\dot{W} = \rho T_0 \dot{s}_p, \tag{12}$$

The mechanical energy ΔW dissipated per cycle of vibration in a medium of volume V is

$$\Delta W = \rho T_0 \int_V \Delta s \, \mathrm{d}V. \tag{13}$$

Equation (13) relates the entropy produced in the material during one cycle of vibration to the elastic energy dissipated.

Finally, the material damping factor γ is defined as the energy dissipated throughout the medium in one cycle, normalized in respect to the maximum elastic energy stored during that cycle [35]:

$$\gamma = \Delta W/4\pi \int_V W_{e1} \, \mathrm{d}V. \tag{14}$$

The modal damping factor ζ is defined [35] as

$$\zeta = \sqrt{\gamma^2(4 + \gamma^2)}. \tag{15}$$

Equations (1)–(15) show the relationships between the stress field and the material or the modal damping factor of the bar due to the thermoelastic effect.

3. THE ELLIPSOIDAL CAVITY IN AN ISOTROPIC MEDIUM

It has been observed in problems of materials with cavities that qualitative results can be obtained by using simple geometries for which analytical solutions are possible. Such analysis yields adequate results for the effect of the concentration of the cavities and additionally it accounts for the effect of their true shape.

To improve understanding of the mechanism of energy conversion and the relation of the cyclic stresses to the vibration damping, analytical and experimental work on porous metals had been carried out. The material cavity, shown in Figure 1, was modelled as a triaxial ellipsoidal cavity with semi-axes a, b and c in the center of an elastic, isotropic and homogeneous unbounded medium. It is assumed that the body at infinity is in a uniform state of stress, the principal directions of which are parallel to the axes of the cavity. The Cartesian co-ordinate axes are chosen to be coincident with the axes of the ellipsoid. Then the stress field at infinity is characterized by

$$\sigma_{xx} = \sigma_1, \qquad \sigma_{yy} = \sigma_2, \qquad \sigma_{zz} = \sigma_3, \qquad \tau_{xy} = \tau_{yz} = \tau_{zx} = 0, \tag{16}$$

where σ_{xx}, σ_{yy} and σ_{zz}, are arbitrarily prescribed principal stresses. The problem to be solved at present consists of the determination of the normal stress distribution induced by the given loading at infinity. The surface of the cavity must be free of boundary stresses. In the absence of body forces, the problem is equivalent to establishing a displacement field $[u, v, w]$, which satisfies the equations of equilibrium (16), and gives rise to an associated field of stress

$$[\Delta u, \Delta v, \Delta w] - 1/(2v - 1) \operatorname{grad} e = 0, \qquad e = \operatorname{div}[\mathrm{u, v, w}], \tag{17}$$

$$\sigma_{xx} = 2vG/(1 - 2v)\,\mathrm{e} + 2G\partial u/\partial x, \ldots, \qquad \tau_{yz} = G(\partial w/\partial y + \partial v/\partial z), \ldots, \tag{18, 19}$$

which conforms to conditions (16) at infinity, while leaving the internal boundary of the ellipsoidal cavity free from the surface tractions. In order to render the boundary conditions for the surface of the cavity manageable curvilinear co-ordinates are introduced.

According to Sadowsky and Sternberg [36], the shape of the internal boundary suggests the use of ellipsoidal co-ordinates. The corresponding co-ordinate transformation, which relates the Cartesian co-ordinates x, y and z to the ellipsoidal co-ordinates $\alpha_i (i = 1, 2, 3)$ is most conveniently introduced with the aid of Jacobian elliptic functions sn α_i, cn α_i, and

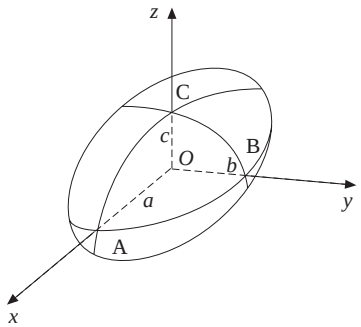

Figure 1. The ellipsoidal cavity in Cartesian co-ordinates.

dn α_i ($i = 1, 2, 3$) [36]. Let

$$s_1 = 1/(k \text{ sn } \alpha_1), \qquad s_2 = 1/\text{dn } (\alpha_2, k'), \qquad s_3 = \text{sn } \alpha_3, \tag{20a}$$

$$c_1 = \text{dn } \alpha_1/(\text{i}k \text{ sn } \alpha_1), \qquad c_2 = -\text{i}k' \text{ sn } (\alpha_2, k')/\text{dn } (\alpha_2, k'), \qquad c_3 = \text{cn } \alpha_3, \tag{20b}$$

$$d_1 = \text{cn } \alpha_1/(\text{i sn } \alpha_1), \qquad d_2 = k' \text{ cn } (\alpha_2, k')/\text{dn } (\alpha_2, k'), \qquad d_3 = \text{dn } \alpha_3. \tag{20c}$$

The co-ordinate transformation from ellipsoidal to cartesian co-ordinates may now be written as

$$x = kms_1s_2s_3, \qquad y = -(km/k')c_1c_2c_3, \qquad z = \text{i}m/(kk')d_1d_2d_3, \tag{21a–c}$$

where the moduli k, and k' and the parameter m are related to the semi-axes of the ellipsoidal cavity a, b and c as follows:

$$k = \sqrt{[(a^2 - b^2)/(a^2 - c^2)]}, \qquad k' = \sqrt{(1 - k^2)}, \qquad m = \sqrt{(a^2 - b^2)}, \tag{22}$$

and where, also without loss of generality, a, b and c are assumed to be ordered by

$$0 < c < b < a. \tag{23}$$

For

$$0 < a_1 \leqslant K, \qquad 0 \leqslant a_2 \leqslant K', \qquad 0 \leqslant a_3 \leqslant K \tag{24}$$

where $4K$ and $2\text{i}K'$ are the real and imaginary periods corresponding to the modulus k, the first octant of the Cartesian space is covered. If α_1^0 is chosen such that

$$s_1^0 \equiv 1/(k \text{ sn } \alpha_1^0) = a/m, \tag{25}$$

it is confirmed that the ellipsoid $\alpha_1 = \alpha_1^0$ has semi-axes a, b and c and coincides with the surface of the cavity, which accounts for the form of equations (22).

The complete solution of the stress problem in ellipsoidal co-ordinates is now extracted directly from reference [36]; see equations (36), (42–46), (49) and (50, 51) on pp. 152–154. In order for these equations to be applicable, several intermediate steps must be taken.

For each point (x, y, z) in the body, equation (21) are solved for the Jacobian elliptic functions sn α_i, cn α_i, dn α_i. Next, from known values of Jacobian elliptic functions sn α_i, cn α_i, and dn α_i the problem of finding the arguments α_i, $i = 1,2,3$, 1^0 must be solved. The solution of this problem is achieved by inverse interpolation in the tables of Jacobian elliptic functions [37] and Chebychev polynomials of fourth degree [38]. Then, with known values of k and k', the complete elliptic integrals K and E are found, from reference [39, 17.3.34, 17.3.36, 17.6.4], to yield the quotient E/K. The zeta functions of Jacobi are then found by interpolation for known values of moduli and arguments α_i, $i = 1$, 1^0. The complete elliptic integral E can now be found from the following equation [39].

$$\text{E} = \text{Z} + \alpha \text{ E/K}. \tag{26}$$

The complete procedure is presented in reference [40].
One can now define

$$0 < \rho_1 = b/a < 1, \qquad 0 < \rho_2 = c/b < 1. \tag{27}$$

As the square $0 \leqslant \rho_1 < 1$, $0 \leqslant \rho_2 \leqslant 1$ is traversed, the ellipsoidal cavity assumes all possible shapes. The invariants of the stress tensor thus calculated are applied to equations (10)–(15) to yield analytical values for damping. Specifically, the normal stresses yield the hydrostatic stress σ_{kk} [26]. For a loading assumed to be time-harmonic, the stress is harmonic $\sigma = \sigma_0 \, \text{e}^{\text{i}\omega t}$ and the heat rate $q(r,t)$ generated due to the thermoelastic effect is

$$q(r,t) = -\alpha_1 T_0(\partial\sigma_{kk}/\partial t) = -\alpha_1 T_0 \, \text{i}\omega \, \text{e}^{\text{i}\omega t}\sigma_{kk0}, \tag{28}$$

where the subscript zero is the stress designated amplitude, ω is the frequency of oscillation of the external load and t is the time. Under this assumption the transient heat conduction equation with heat generation in cylindrical co-ordinates can be written in the form

$$\partial^2 T/\partial r^2 + 1/r\partial T/\partial r + \partial^2 T/\partial z^2 + q(r,t)/k = a_{diff}\partial T/\partial t, \tag{29}$$

where $q(r, t)$ is the rate of heat generation term, k is the thermal conductivity and α_{diff} is the thermal diffusivity. Since σ_{kk} is time-harmonic and linearity is assumed, the fluctuations in T will necessarily be time-harmonic; therefore T can be assumed to be

$$T(r,t) = T_m(r)\, \mathrm{e}^{\mathrm{i}\omega t}. \tag{30}$$

Equations (28–30) yield

$$\partial^2 T_m/\partial r^2 + 1/r\partial T_m/\partial r + \partial^2 T_m/\partial z^2 - \alpha_1 T_0\, \mathrm{i}\omega\, \mathrm{e}^{\mathrm{i}\omega t}\sigma_{kk}/k = a_{diff}\partial T_m/\partial t. \tag{31}$$

Because T_m is a complex number, $T_m = \mathrm{Re}\{T_m\} + \mathrm{i}\,\mathrm{Im}\{T_m\}$, equation (31) yields the following two equations:

$$\partial^2\,\mathrm{Re}(T_m)/\partial r^2 + 1/r\partial\,\mathrm{Re}(T_m)/\partial r + \partial^2\,\mathrm{Re}(T_m)/\partial z^2 + \omega/a_{diff}\,\mathrm{Im}(T_m) = 0, \tag{32}$$

$$\partial^2\,\mathrm{Im}(T_m)/\partial r^2 + 1/r\partial\,\mathrm{Im}(T_m)/\partial r + \partial^2\,\mathrm{Im}(T_m)/\partial z^2 - \omega/a_{diff}\,\mathrm{Re}(T_m) = \alpha_1 T_0\omega\sigma_{kk}/k. \tag{33}$$

The temperature field is derived as the solution of differential equations (32, 33) and the boundary conditions

$$\partial T/\partial r = 0, \qquad \text{at} \quad r = R_2, \quad z = 0, H/2, \tag{34}$$

where R_2 is the outer radius of the cylinder and $H = 2R_2$ is the height of the cylinder. It is assumed that the flow of heat from the solid towards the cavity is zero, because the heat transfer from the solid to the cavity can be neglected due to the low thermal conductivity and the limited thermal capacity. The temperature field is computed as the solution of equations (32) and (33) with the boundary conditions (34). This was done by replacing the system of equations (32) and (33) by a system of finite difference equations and solving the resulting system of linear equations, including the boundary conditions.

The mechanical energy ΔW dissipated in the solid per cycle of vibration is derived from equations (9), (11), (13), with temperatures calculated from the solution of equations (32)–(34) above. Since the temperatures $T_{i,j}$ have been computed by a finite difference method at a lattice of points (i, j), the integration is replaced with summation, by using the trapezoidal rule:

$$\Delta W = k\pi T_p/2T_0\left[H/2/\mathrm{dr}\sum_{i=1}^{n}(T_{i+1,j} - T_{i-1,j})^2 r_{i,j} + \mathrm{dr}/\mathrm{dz}\sum_{i=1}^{n}(T_{i,j+1} - T_{i,j-1,})^2 r_{i,j}\right] \tag{35}$$

where $T_p = \omega/2\pi$ is the period of vibration and dr and dz are the mesh spacings in the r and z axes.

By using the relationships among the invariants of the stress tensor, the energy of elastic deformation W_{el} stored per unit volume and cycle is derived from equation (10) as

$$W_{el} = (1/2E)\sigma_{kk}^2 - (1 + \nu)/E(\sigma_{rr}\sigma_{zz} + \sigma_{zz}\sigma_{\theta\theta} + \sigma_{\theta\theta}\sigma_{rr}). \tag{36}$$

The total energy elastic $W_{elastic}$ of elastic deformation per cycle in the volume V of the solid is

$$W_{elastic} = \int_V W_{e1}\, \mathrm{d}V \tag{37}$$

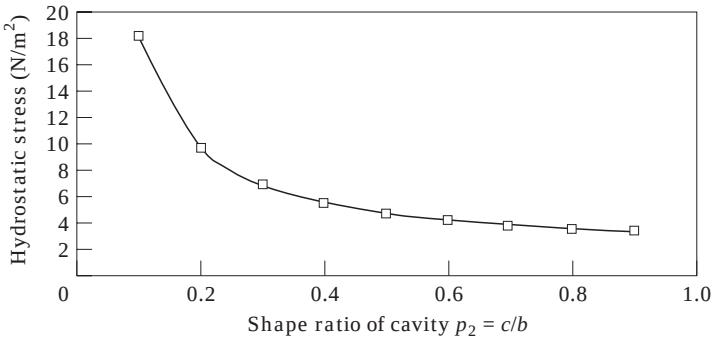

Figure 2. Hydrostatic stress as a function of the shape ratio $p_2 = c/b$; analytical results. Shape ratio of cavity, $p_1 = b/a = 0{\cdot}99$.

Assuming that the stress concentration diminishes as one moves away from the ellipsoidal cavity, one can superpose the stress fields in a lattice of ellipsoidal cavities and integrate over the volume, thus deriving the damping factor from equations (14) and (35)–(37).

A numerical application was performed for cavity spacing $2R_2 = 0{\cdot}0016$ m and $H = 2R_2$. The lattice spacing of the cavities was assumed to be uniform, $H = 2R_2$. For different shape ratios $\rho_2 = c/b$, $\rho_1 = b/a = 0{\cdot}999$, load at infinity $S = 1$ N/m^2 and the same stress oscillation frequency ω, the hydrostatic stress at point B shown in Figure 1 and corresponding to x, $y = 0$, $y = b$, is plotted against the shape ratio c/b in Figure 2. It can be seen that σ_{kk} increases exponentially with decreasing c/b, as anticipated due to the stress concentration. From reference [31, article 122, p. 359], the following values are anticipated for a spherical cavity, which corresponds to $\rho_1 = \rho_2 = 1{:}\sigma_{kk} = 2{\cdot}59$, $\sigma_z = 2{\cdot}07$. Additionally, the stress distribution is independent of the absolute values of the semi-axes a and b taken on the axes x and y respectively, given of course that the load at infinity is parallel to the z-axis of the cylindrical co-ordinate system. For different void ratios Void $(\%) = (V_1/V_2) = 2/3\ a\ b\ c/R_2^3\ 100$, occurring from different shape ratios $\rho_2 = c/b$, as in Figure 2 the analytically calculated material thermodynamic damping factor (MDF) is plotted against Void in Figure 3. It is apparent that damping increases with decreasing shape ratio $\rho_2 = c/b$, and consequently with increasing stress concentration as expected. Damping also increases with increasing Void.

4. EXPERIMENTAL STUDY

On the basis of the analytical results shown in Figures 2 and 3, it is apparent that the damping change due to the existence of porosity in the metal will be substantial. To test this hypothesis, changes in modal damping were evaluated experimentally. Tests have been performed on four metallic bars made out of 316-L stainless steel with varying porosity. The porous material was a product of Mott Metallurgical Corporation with the commercial designation: Mott porous 316L SS sheets, series 1100 with Micron Grades 0·5, 40 and 100 for porosities 25%, 50% and 60% respectively

The physical characteristics of the bars were as presented in Table 1. The first natural frequency was calculated for bar 1. Then the lengths of bars 2, 3 and 4 were selected, as shown in Table 1, to have the same first natural frequency.

The experimental set-up is shown in Figure 4. Each bar had one fixed and one free end. An accelerometer of 1 g mass was fixed on the free end of the bar. The bar was set into free vibration from the initial position by hitting it with a hammer in the z-direction. The

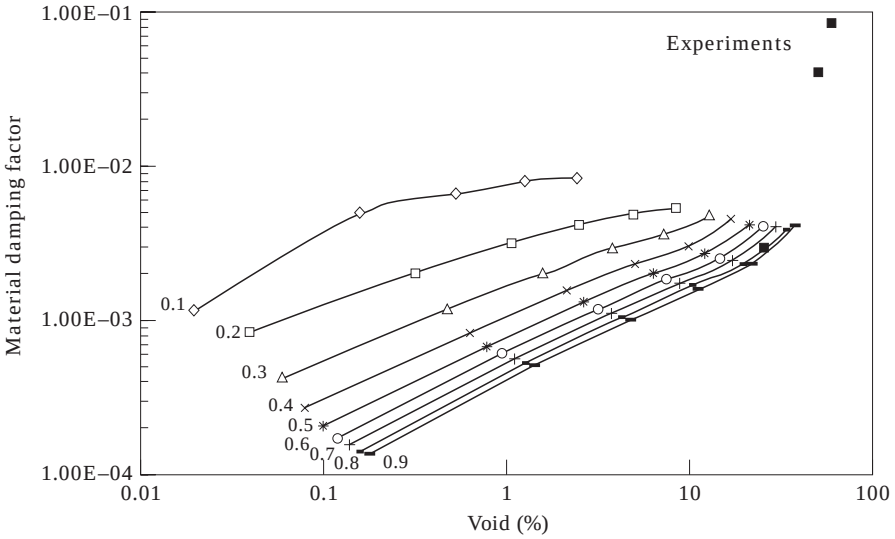

Figure 3. The material damping factor versus Void (%); ■, experimental results; c/b values for analytical results: –◇–, 0·1; –□–, 0·2; –△–, 0·3; – × –, 0·4; –∗–, 0·5; –○–, 0·6; – + –, 0·7; – ▬ –, 0·8; –■–, 0·9.

metal response was measured directly at the same position, through the accelerometer. The output of the latter after amplification was introduced through a Data Acquisition Card (Omega OMB-DAQBOOK-100/-120/-200) to a PC computer and stored for further analysis. The sampling frequency was 3–5 kHz.

The vibration Modal Damping Factor ζ (MDF) was obtained by applying the logarithmic decrement method [35]. Ten measurements of damping have been performed

TABLE 1

Physical characteristics of measured bars; experimental results

Bar	Porosity (%)	Length (m)	Width (m)	Height (m)	Young's modulus ($N/m^2 \times 10^{11}$)	Density (kg/m^3)	Natural frequency (Hz)	Measured damping factor
1	0	0·3048	0·031	0·003175	2·0	7860	28	
2	25	0·25	0·031	0·003175	0·517	5895	28	0·003
3	50	0·17	0·031	0·003175	0·158	3930	28	0·04
4	60	0·19	0·031	0·003175	0·151	3144	28	0·085

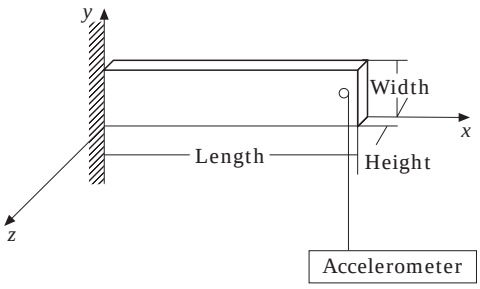

Figure 4. The experimental set-up.

on each bar. Their average was used to yield the difference between the measured damping of the porous bar and the measured damping of the non-porous bar. This difference accounts for the porosity only and was compared with the analytical results in the same sense.

4. CONCLUSIONS

The thermodynamic theory of damping was used to find the material damping due to the material porosity, which results in an additional damping mechanism due to the non-reversible flow of heat from areas of higher heat generation to others of lower heat generation.

The analysis and experiments have been limited to elastic strains and low frequencies, leading to the production of change in the apparent material damping factor which depends on the porosity and thus becomes a material *and* a system property.

Solutions for the infinite solid with an ellipsoidal cavity and constant hoop stress in one direction only at infinity and a regular lattice of equidistant ellipsoidal cavities in a rectangular arrangement were employed. Since the additional damping is due to the stress concentration at the ellipsoidal surface, the assumption was made that one was interested in small cavities only, as compared with the cavity spacing; thus the effect of the stress at one cavity upon the stress in the vicinity of another cavity can be neglected. A finite difference scheme was used to solve the heat conduction equation along well-known lines. The apparent material damping factor was computed by numerical integrations.

The stress concentration increases as the ellipticity ratio c/b in the direction of the hoop stress becomes smaller, as shown clearly in Figure 2. The damping factor consequently increases, as shown in Figure 3. Moreover, increasing Void leads, in the range considered, to higher damping action.

The stress field about an ellipsoidal cavity in the elastic space with constant stress in one direction at infinity does not depend on the cavity dimensions: for a very small void ratio one would expect very little increase in the apparent damping due to the cavities. It is the interaction, less the stress and more the thermal, that causes the apparent material damping factor to increase substantially with the void ratio. Thus, in Figure 3 one observes a nearly linear relationship between the additional material damping factor and void ratio for low void ratios. For higher void ratios, above about 25%, damping starts increasing more rapidly.

We have not found a material to conform exactly with the model that we used in the analysis. The commercially available material that we have found had nearly ellipsoidal cavities not in a regular spacing but, rather, at random. Moreover, some cavities were connected, although most were of elliptical shape. Only materials with three different values of the void ratio were available and they were of high ratios, 25%, 50% and 60%. Above 40% void ratio, analysis is problematic because the ellipsoidal cavities come very close to one-another and, in addition to the questionable validity of our assumptions, the numerical solution seems to be progressively more inaccurate. However, superposition of the analytical and experimental results showed that the latter agree with the analytical/numerical results for lower values of the void ratio, but that they become higher, for higher void ratios.

This analysis can be used in a number of engineering problems: (1) as a continuous quality control tool for the production of ceramics, glass and similar materials such that their quality is diminished with even small porosity; (2) as a design tool for the increasing use of porous materials for reduction of the structure borne noise in automotive, aircraft

and other applications; (3) in the biomedical field, as part of diagnostic and monitoring tools for osteoporosis and other conditions of bone loss in the form of increasing porosity.

ACKNOWLEDGMENTS

The help of Dr Norman Katz, Professor in The Systems, Science and Mathematics Department of Washington University in St. Louis, U.S.A. in the selection of the appropriate interpolation technique in the tables of Jacobian elliptic functions, is greatly appreciated.

REFERENCES

1. B. J. Lazan 1968 *Damping of Materials and Members in Structural Mechanics*. Oxford: Pergamon Press.
2. C. Zener 1937 *Physical Review* **52**, 230–235.
3. M. Biot 1956 *Journal of Applied Physics* **27**, 240–253.
4. K. Lucke 1956 *Journal of Applied Physics* **27**, 1433–1438. Ultrasonic attenuation caused by thermoelastic heat flow.
5. H. Deresiewitcz 1957 *Journal of the Acoustical Society of America* **29**, 204–209. Plane waves in a thermoelastic solid.
7. J. Alblas 1961 *Applied Scientific Research* **10**(Section A), 349–367. On the general theory of thermo-elastic friction.
7. J. Alblas 1981 *Journal of Thermal Stresses* **4**, 333–355. A note on the theory of thermoelastic damping.
8. W. Gillis 1968 *Technical Memorandum X*-53722, *George C. Marshall Space Flight Center*, *Orbital Mechanics Section*. Damping of thermoelastic structures.
9. J. Tasi 1963 *Journal of Applied Mechanics* **30**, 562–567. Thermoelastic dissipation in vibrating plates.
10. J. Tasi and G. Hermann 1964 *Journal of the Acoustical Society of America* **36**, 100–110.
11. R. Shieh 1971 *NASA TND*-6448, *NASA Langley Research Center*, *Hampton*, *Virginia*. Thermoelastic damping and its effect on flutter of stressed panels situated in a supersonic airflow.
12. R. Shieh 1975 *Transactions of the American Society of Mechanical Engineers*, *Journal of Applied Mechanics* **42**, 405–410 Thermoelastic vibration and damping for circular Timoshenko beams.
13. R. Shieh 1979 *Transactions of the Americal Society of Mechanical Engineers*, *Journal of Applied Mechanics* **46**, 169–174. Eigensolutions for coupled thermoelastic vibrations of Timoshenko beams.
14. U. Lee 1985 *American Institute of Aeronautics and Astronautics Journal* **23**, 1783–1790. Thermoelastic and electromagnetic damping analysis.
15. L. Goodman, C. Chang and A. Robinson 1962 *Technical Documentary Report No*. *ASD-TDR*-62-1031, *Wright–Patterson Air Force Base*, *Ohio*. Thermoelastic damping.
16. L. Landau and E. Lifshitz 1986 *Theory of Elasticity* New York: Pergamon Press.
17. B. Armstrong 1984 *Geophysics* **49**, 1032–1040. Models for thermoelastic attenuation of waves in heterogeneous solids.
18. V. Kinra and K. Milligan 1994 *Transactions of the Americal Society of Mechanical Engineers Journal of Applied Mechanics* **61**, 71–76. A second law analysis of thermoelastic damping.
19. K. Milligan and V. Kinra 1993 *Mechanics Research Communications* **20**, 137–142. On the thermoelastic damping of a one-dimensional inclusion in a uniaxial bar.
20. J. Bishop and V. Kinra 1992 in *Mechanics and Mechanisms of Material Damping*, *ASTM STP* 1169 (V. K. Kinra and A. Wolfenden editors), 457–470. Some improvements in the flexural damping measurement technique. Philadelphia, PA: American Society for Testing and Materials.
21. J. Bishop and V. Kinra 1993 *Journal of Reinforced Plastics and Composites* **12**, 210–226. Thermoelastic damping of a laminated beam in flexure and extension.
22. J. Bishop and V. Kinra 1993 *Thermodynamics and the Design and Improvement of Energy Systems*, *AES-Vol*. 30, *HTD-Vol*. 266 (H. J. Richter, editor), *Proceedings of the* 1993 *Winter Annual Meeting*, 127–138. Elastothermodynamic damping of metal–matrix composites.

23. K. Milligan and V. Kinra 1993 *Thermodynamics and the Design and Improvement of Energy Systems*, *AES-Vol*. 30, *HTD-Vol* 266 (H. J. Richter, editor), *Proceedings of the* 1993 *Winter Annual Meeting*, 139–148. Elastothermodynamic damping of fibre reinforced metal–matrix composites.
24. M. Zemansky and R. Dittman 1981 *Heat and Thermodynamics*, New York: McGraw-Hill; sixth edition.
25. D. Frederick and T. S. Chang 1972 *Continuum Mechanics*. Cambridge, MA; Scientific Publishers, See p. 169.
26. W. Nowacki 1962 *Thermoelasticity*. Oxford: Pergamon Press.
27. M. N. Ozisik 1993 *Heat Conduction*. New York: John Wiley; second edition.
28. J. Bishop and V. K. Kinra 1994 *AES-Vol*. 33, *ASME*, Elastothermodynamic damping in particle-reinforced metal-matrix composites.
29. B. D. Coleman and W. Noll 1961 *Reviews of Modern Physics*, **33**, 239–249. Foundations of linear viscoelasticity.
30. B. D. Coleman and V. J. Mizel 1964 *Journal of Chemistry and Physics* **40**, 1116–1125. Existence of caloric equations of state thermodynamics.
31. S. Timoshenko and J. N. Goodier 1951 *Theory of Elasticity*. New York: McGraw-Hill; second edition.
32. A. Bejan 1982 *Entropy Generation Through Heat and Fluid Flow*. New York: John Wiley.
33. M. Gouy 1889 *Journal of Physics* **8**, 501. Sur l'energie utilisable.
34. A. Stodola 1910 *Steam and Gas Turbines*. New York: McGraw Hill.
35. A. Dimarogonas 1996 *Vibration for Engineers*. Englewood Cliffs, NJ: Prentice Hall; second edition.
36. M. A. Sadowski and E. Sternberg 1949 *Journal of Applied Mechanics*, Paper No. 48—A-29. Stress concentration around a triaxial ellipsoidal cavity.
37. L. M. Milne-Thomson 1950 *Jacobian Elliptic Function Tables*. New York. Dover.
38. K. Atkinson 1993 *Elementary Numerical Analysis*. New York: John Wiley; second edition
39. M. Abramowitz and I. A. Stegun *Handbook of Mathematical Functions*. New York: Dover.
40. S. D. Panteliou, A. Dimarogonas and I. N. Katz 1996 *Computers and Mathematical Applications* **32**, 51–57. Direct and inverse interpolation for Jacobian elliptic functions, zeta functions of Jacobi and complete elliptic integrals of the second kind.